Journal of Power Sources 196 (2011) 1730–1737

Contents lists available at ScienceDirect

Journal of Power Sources

journal homepage: www.elsevier.com/locate/jpowsour

Ethanol oxidation reaction activity of highly dispersed Pt/SnO_2 double nanoparticles on carbon black

Eiji Higuchi*, Kazumasa Miyata, Tomonori Takase, Hiroshi Inoue*

Department of Applied Chemistry, Graduate School of Engineering, Osaka Prefecture University, Sakai, Osaka 599-8531, Japan

ARTICLE INFO

Article history:
Received 3 August 2010
Received in revised form
28 September 2010
Accepted 1 October 2010
Available online 8 October 2010

Keywords:
$Pt/SnO_2/CB$
Ethanol oxidation
Electrocatalyst
Nanoparticle

ABSTRACT

Highly dispersed Pt and SnO_2 double nanoparticles containing different Pt/Sn ratios (denoted as $Pt/SnO_2/CB$) were prepared on carbon black (CB) by the modified Bönnemann method. The average size of Pt and SnO_2 nanoparticles was 3.1 ± 0.5 nm and 2.5 ± 0.3 nm, respectively, in $Pt/SnO_2(3:1)/CB$, 3.0 ± 0.5 nm and 2.6 ± 0.3 nm, respectively, in $Pt/SnO_2(1:1)/CB$, and 2.8 ± 0.5 nm and 2.5 ± 0.3 nm, respectively, in $Pt/SnO_2(1:3)/CB$. The $Pt/SnO_2(3:1)/CB$ electrode showed the highest specific activity and lowest overpotential for ethanol oxidation reaction (EOR), and was superior to a Pt/CB electrode. Current density for EOR at 0.40 and 0.60 V vs. reversible hydrogen electrode for the $Pt/SnO_2(3:1)/CB$ electrode decayed more slowly than that for the Pt/CB electrode because of a synergistic effect between Pt and SnO_2 nanoparticles. The predominant reaction product was acetic acid, and its current efficiency was about 70%, while that for CO_2 production was about 30%.

1. Introduction

Direct alcohol fuel cells (DAFCs) have attracted much interest as primary power sources for portable electronic devices. The simplest direct methanol fuel cells [1–4] and the direct ethanol fuel cells [5–7] are the most popular DAFCs. In particular, ethanol is a nontoxic fuel that can be easily produced in large quantity by carbon-neutral processes like the fermentation of sugar-containing raw materials, making it attractive for fuel cell vehicles. Pt–M (M = Ru, Rh, Sn) alloys [8–11] and Pt-loaded oxides such as Pt/RuO_2 and Pt/ZrO_2 have been developed to improve the slow ethanol oxidation reaction (EOR). Several authors found that Pt–Sn alloy catalysts was superior to other Pt-based alloy catalysts on EOR activity [12,13]. Lamy et al. prepared bimetallic Pt–Sn catalysts on carbon black (CB) having high EOR activity [14]. Ribeiro et al. recently reported that $Pt_{79}Sn_{21}/CB$ and $Pt_{68}Sn_9Ir_{23}/CB$ catalysts promoted the ethanol oxidation at a potential of *ca.* 0.25 V vs. reversible hydrogen electrode (RHE) [15].

Carbon-supported Pt-based alloy nanoparticles are usually prepared by impregnation methods [16] and microemulsion methods [17], followed by heating. However, heat treatment often causes the sintering of metal particles, leading to a decrease in EOR activity. Other preparation methods use colloids [18–21] and nanocapsules [22] but the resultant nanoparticles are large in size and exhibit broad size distributions. Hence, controlling the particle size and its distribution, in addition to alloy composition, would significantly improve the EOR activity, in particular the mass activity. Bönnemann et al. successfully prepared bimetallic particles with average particle sizes smaller than 2 nm and narrow size distributions in THF at room temperature [23,24]. Tetraalkylammonium ions NR_4^+ ions (R = C_4–C_{20}), which acted as stabilizers, covered the bimetallic particles, providing a promising method to control particle size and size distribution. Bönnemann et al. have also successfully prepared bimetallic Pt–Sn nanoparticles [25]. Our original plan was to prepare similar bimetallic Pt–Sn nanoparticles with an appropriate particle size and narrow distribution as electrocatalysts for EOR. Instead, we partly modified the Bönnemann's method and obtained Pt/SnO_2 double nanoparticles.

Some research groups have recently reported that Au/CeO_2 and Au/TiO_2 double nanoparticles showed high activity for the water–gas shift reaction although bulk Au and metal oxides were inactive [26–28]. Rodriguez et al. found that high activity of Au nanoparticles partially covered by CeO_2 or TiO_2 nanoparticles resulted from a synergistic effect of the Au and CeO_2 or TiO_2 nanoparticles based on direct participation of the oxide–Au interface [28]. In this case, oxygen vacancies of the oxide nanoparticles accelerated the dissociation of water, which was otherwise difficult on Au nanoparticles. The contact between oxide and noble metal nanoparticles were therefore crucial in enhancing the catalytic activity. Therefore, the Pt/SnO_2 double nanoparticles are expected to improve EOR activity compared to previous Pt/SnO_2 bulk powder catalysts. In the present study, we characterized the Pt/SnO_2 double nanoparticles by spectroscopic methods and evaluated their electrocatalytic activity for EOR and durability.

* Corresponding authors. Tel.: +81 72 254 9319; fax: +81 72 254 9319.
E-mail address: e-higuchi@chem.osakafu-u.ac.jp (E. Higuchi).

0378-7753/$ – see front matter © 2010 Published by Elsevier B.V.
doi:10.1016/j.jpowsour.2010.10.008

2. Experimental

2.1. Preparation of $Pt/SnO_2/CB$ and Pt/CB catalysts

$N(Oct)_4(BEt_3H)$ was prepared according to literature [25]. A solution of 0.3 M $N(Oct)_4(BEt_3H)$ (12 mL) in THF was added dropwise to a vigorously stirred solution containing $PtCl_2$ (0.177 g, 0.67 mmol) and $SnCl_2$ (0.043 g, 0.23 mmol) at 30 °C in an Ar atmosphere. The reaction mixture was stirred for 3 h, resulting in a black colloidal $Pt_3Sn[N(Oct)_4Cl]_8$ suspension [25]. Acetone (15 mL) was added into the suspension, followed by stirring for 30 min to oxidize any excess $N(Oct)_4(BEt_3H)$. The suspended $Pt_3Sn[N(Oct)_4Cl]_8$ was isolated by suction filtration in air and dried in vacuo for 16 h at room temperature, yielding a black, waxy solid. Exposure to air during the filtration, which was not in the original method, can lead to the oxidation of Sn.

The black solid was redispersed in ethanol. Ketjen black (67 mg) was added in the dispersion and sonicated for 10 min. After suction filtration, a residual black powder (powder (A)) was collected and heat-treated at 200 °C in air for 30 min to remove $N(Oct)_4Cl$. The resultant powder was called $Pt/SnO_2(3:1)/CB$.

$Pt/SnO_2(9:1)/CB$, $Pt/SnO_2(1:1)/CB$, $Pt/SnO_2(1:3)/CB$, Pt/CB, and SnO_2/CB powders were also prepared by the similar procedure except for different Pt/Sn molar ratios.

2.2. Characterization of $Pt/SnO_2/CB$ and Pt/CB catalysts

Thermogravimetric (TG) analysis was performed in air using a Thermo Plus TG8120 apparatus (Rigaku) by heating from room temperature to 500 °C at a rate of 1 K min^{-1}. Microstructure of $Pt/SnO_2(3:1)/CB$ was examined by field-emission transmission electron microscopy (FE-TEM, Hitachi). FE-TEM specimens were prepared by pipetting a drop of an ethanol dispersion of each catalyst onto a collodion-coated copper grid and evaporating ethanol. Size distribution of Pt and SnO_2 nanoparticles were measured for 500 Pt and 100 SnO_2 nanoparticles randomly chosen from high resolution TEM images. Structural analysis for $Pt/SnO_2(9:1)/CB$, $Pt/SnO_2(3:1)/CB$, $Pt/SnO_2(1:1)/CB$, $Pt/SnO_2(1:3)/CB$, Pt/CB, and SnO_2/CB catalysts was performed using an X-ray diffractometer (Shimadzu XRD-6100) equipped with a Cu Kα source (λ = 0.1541 nm, 50 kV, 30 mA, 4 K min^{-1}). Chemical state of Pt and Sn in each catalyst was measured by X-ray photoelectron spectroscopy (XPS) using a photoelectron spectrometer (ESCA-3200, Shimadzu). The X-ray source was Mg Kα with 1253.6 eV operating at 8 kV and 30 mA. The base pressure of the system was 1.3×10^{-7} Pa. The Pt/Sn molar ratio of $Pt/SnO_2(9:1)/CB$, $Pt/SnO_2(3:1)/CB$, $Pt/SnO_2(1:1)/CB$, $Pt/SnO_2(1:3)/CB$, Pt/CB, and SnO_2/CB catalysts was investigated by energy dispersive X-ray analysis (EDX).

2.3. Electrochemical measurements

To achieve ultrathin and uniform dispersion of $Pt/SnO_2(9:1)/CB$, $Pt/SnO_2(3:1)/CB$, $Pt/SnO_2(1:1)/CB$, $Pt/SnO_2(1:3)/CB$, Pt/CB, and SnO_2/CB catalysts on a glassy carbon (GC) substrate of ϕ5 mm, the following procedure was used [29]. Briefly, each catalyst powder (6.28 mg) was dispersed in ethanol (50 mL, Wako) and sonicated for 10 min. The resultant dispersion (20 μL) was cast on a GC substrate and dried overnight. The amount of $Pt/SnO_2/CB$, Pt/CB and SnO_2/CB catalysts in the suspension was adjusted to $w_{CB} = 5.5\ \mu g\ cm^{-2}$ (w_{CB}: amount of CB loaded on GC), while the amount of Pt/SnO_2 loaded on the GC (w_{Pt/SnO_2}) was 12.8 μg cm^{-2}. A 0.05 wt% Nafion solution (Aldrich) in ethanol (10 μL) was cast on the dried catalyst layer, and then heat-treated in air at 120 °C for 1 h to evaporate ethanol, resulting in a catalyst electrode thinly coated with a thin Nafion film of 0.1 μm. A rotating disk electrode (RDE) apparatus (RED-1, Nikko Keisoku) equipped with a gas-tight Pyrex glass cell was used to measure electrochemical properties of the $Pt/SnO_2(9:1)/CB$, $Pt/SnO_2(3:1)/CB$, $Pt/SnO_2(1:1)/CB$, $Pt/SnO_2(1:3)/CB$, Pt/CB, and SnO_2/CB electrodes. A Pt plate and an RHE electrode were used as the counter and reference electrodes, respectively. EOR activity and durability of each electrode were evaluated at 30 °C by cyclic voltammetry (CV) and potentiostatic electrolysis. In CO-stripping voltammetric measurements, CO was adsorbed on each electrode by immersing in a 0.5 M H_2SO_4 solution saturated with CO for 15 min at a constant potential of 0.05 V vs. RHE. The excess CO was eliminated by Ar bubbling, and stripping charge was evaluated from a voltammogram between 0.05 and 1.0 V vs. RHE at a sweep rate of 50 mV s^{-1}.

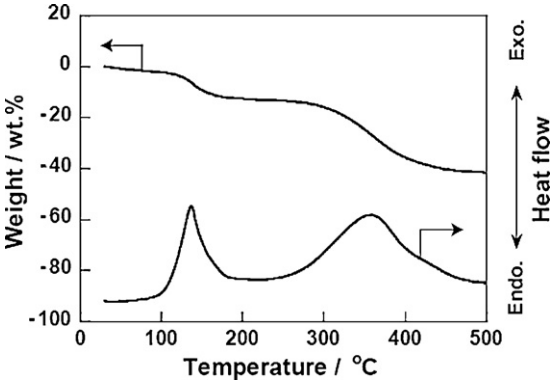

Fig. 1. TG–DTA curves of black powder (A).

2.4. Measurement of reaction products

Products in potentiostatic electrolysis with the $Pt/SnO_2(3:1)/CB$ electrode were qualitatively and quantitatively analyzed by a high performance liquid chromatograph (HPLC, Tosoh) with an UV detector (UV-8020) for acetic acid and acetaldehyde and a gas chromatograph (GC, Shimadzu GC-14B) with a Porapak Q column for CO_2.

3. Results and discussion

3.1. $Pt/SnO_2/CB$, Pt/CB, and SnO_2/CB catalyst structures

Fig. 1 shows TG–DTA curves for black powder (A). The initial weight loss below 100 °C (*ca.* 2 wt%) was assigned to evaporation of physisorbed water from the powder (A) and the second weight loss observed between 100 and 200 °C is due to oxidation of stabilizer $N(Oct)_4Cl$; this is in agreement with a previous report [30]. The oxidation of CB starts at about 300 °C. Weight losses due to the oxidation of $N(Oct)_4Cl$ and CB were *ca.* 10 and 30 wt%, respectively. Therefore, total content of Pt and SnO_2 loaded in $Pt/SnO_2/CB$ catalysts was evaluated to be *ca.* 67 wt%.

Fig. 2(a) and (b) shows FE-TEM images of the $Pt/SnO_2(3:1)/CB$ catalyst at different magnifications. Fig. 2(a) clearly shows the existence of nanoparticles on CB. In Fig. 2(b) there were two kinds of lattice fringes with interfringe distances of 0.225 and 0.333 nm. These lattice fringes were in close agreement with those of the (1 1 1) plane (0.227 nm) in the face-centered cubic (fcc) Pt crystal and the (1 1 0) plane (0.335 nm) in the tetragonal SnO_2 crystal, respectively, suggesting that Pt and SnO_2 double nanoparticles, instead of Pt_3Sn alloy nanoparticles, are loaded on CB probably because surface Sn atoms in the Pt_3Sn alloy were oxidized and segregated to form SnO_2 nanoparticles. Fig. 2(c) and (d) shows particle size distribution profiles for Pt and SnO_2 nanoparticles, respectively. Average size and standard deviation were 3.1 ± 0.5 nm for

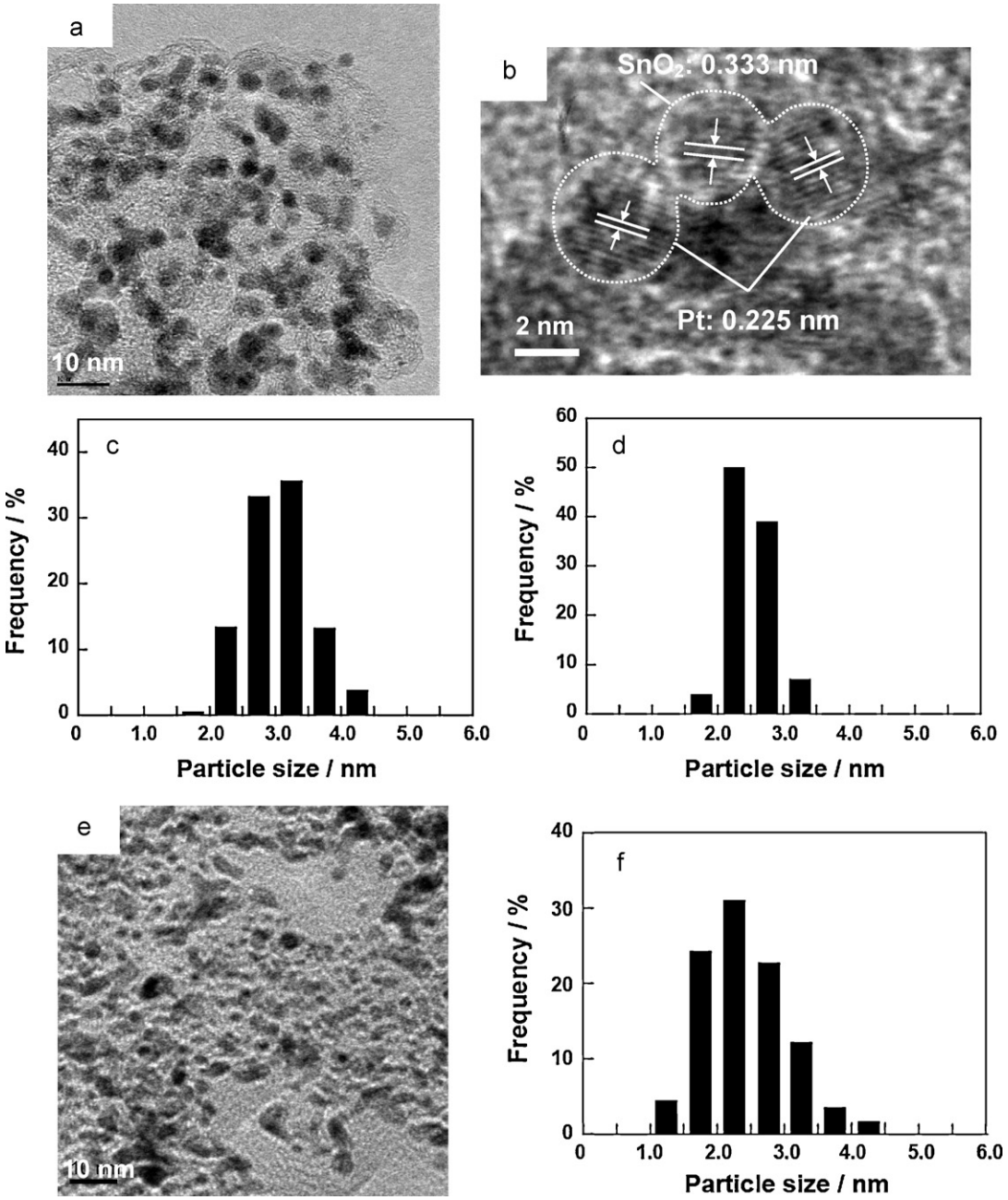

Fig. 2. TEM images of Pt/SnO_2(3:1)/CB catalyst (a) at a magnification of 100,000; (b) at a magnification of 500,000; particle size distribution of (c) Pt and (d) SnO_2 nanoparticles; (e) a TEM image of Pt/CB at a magnification of 100,000; (f) particle size distribution of Pt nanoparticles.

the Pt nanoparticles and 2.5 ± 0.3 nm for the SnO_2 nanoparticles, indicating that size distribution of both nanoparticles was narrow. Average size and standard deviation of other Pt/SnO_2/CB catalysts were also shown in Table 2. Average size of Pt decreased with an decrease of Pt content while that of SnO_2 did not depend on the Pt content.

Fig. 2(e) and (f) shows a TEM image and a size distribution profile of Pt nanoparticles for Pt/CB catalyst, respectively. Fig. 2(e) clearly shows the Pt nanoparticles are loaded on CB. In Fig. 2(f), average size of the Pt nanoparticles was 2.4 ± 0.6 nm. These results indicate that N(Oct)$_4$(BEt_3H) is likely to act not only as a reducing agent, but also as a stabilizer.

Fig. 3 shows XRD patterns for Pt/SnO_2(9:1)/CB, Pt/SnO_2(3:1)/CB, Pt/SnO_2(1:1)/CB, Pt/SnO_2(1:3)/CB, Pt/CB, and SnO_2/CB catalysts. Each XRD pattern exhibit a broad diffraction peak at 20–25°, which was assigned to the (0 0 2) plane of CB with a hexagonal structure. Diffraction peaks at 39.7, 46.2, 67.5, and 81.3° for Pt/CB were assigned to Pt(1 1 1), (2 0 0), (2 2 0), and (3 1 1), respectively; these are characteristic of the fcc structure. Lattice constants were evaluated to be 0.394 and 0.393 nm for Pt/SnO_2(3:1)/CB and Pt/CB catalysts, respectively, which are in good agreement with the lattice constant of Pt (0.3923 nm). The Pt(1 1 1) peak observed for Pt/SnO_2(9:1)/CB, Pt/SnO_2(3:1)/CB, Pt/SnO_2(1:1)/CB, Pt/SnO_2(1:3)/CB, and Pt/CB and the SnO_2(2 1 1) peak displayed by the SnO_2/CB catalyst were used to calculate crystallite sizes according to Scherrer's equation and summarized in Table 1. The average Pt crystallite size for the Pt/SnO_2(3:1)/CB catalyst was 2.9 nm which was in close agreement with the TEM evaluations. The average Pt crystallite size for the Pt/CB catalyst increased from 1.9 nm to *ca.* 3.6 nm during heat-treatment due to sintering. On the other hand,

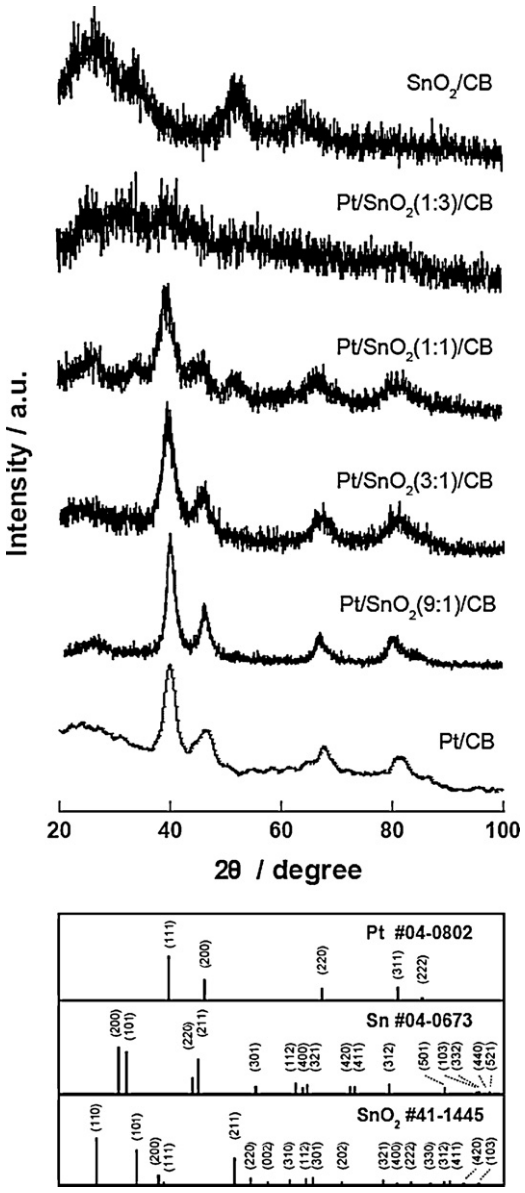

Fig. 3. X-ray diffraction patterns of $Pt/SnO_2(9:1)/CB$, $Pt/SnO_2(3:1)/CB$, $Pt/SnO_2(1:1)/CB$, $Pt/SnO_2(1:3)/CB$, Pt/CB, and SnO_2/CB catalysts.

average SnO_2 crystallite size (2.0 nm) for the SnO_2/CB catalyst was maintained even during heat-treatment.

Contents of Pt and SnO_2 in $Pt/SnO_2(9:1)/CB$, $Pt/SnO_2(3:1)/CB$, $Pt/SnO_2(1:1)/CB$, and $Pt/SnO_2(1:3)/CB$ were evaluated by EDX and summarized in Table 1. The contents of Pt and SnO_2 in each catalyst was nearly equal to those of Pt and Sn precursors. Thus the contents of Pt and SnO_2 loaded on CB can be controlled by those of Pt and Sn precursors.

XPS analyses did not show any peak in N1s and Cl2p core level spectra, suggesting that the heat-treatment completely removed $N(Oct)_4Cl$. Fig. 4 shows Pt4f and Sn3d core level spectra for $Pt/SnO_2(9:1)/CB$, $Pt/SnO_2(3:1)/CB$, $Pt/SnO_2(1:1)/CB$, $Pt/SnO_2(1:3)/CB$, and Pt/CB. Pt4f spectra exhibited intense doublets at 71.1 and 74.4 eV (Fig. 4(a)), which were assigned to metallic Pt (Pt^0), but there was not any peak assigned to Pt oxides. On the other hand, Sn3d spectra (Fig. 4(b)) clearly exhibited intense doublets assigned to the $3d_{3/2}$ (495.1 eV) and $3d_{5/2}$ (486.7 eV) of Sn^{4+} but no doublet of metallic Sn (493.2 and 484.8 eV), thus suggesting that Sn was oxidized to SnO_2.

3.2. Electrochemical properties and EOR activity of $Pt/SnO_2/CB$, Pt/CB, and SnO_2/CB electrodes

Fig. 5 shows cyclic voltammograms of Nafion-coated $Pt/SnO_2(9:1)/CB$, $Pt/SnO_2(3:1)/CB$, $Pt/SnO_2(1:1)/CB$, $Pt/SnO_2(1:3)/CB$, Pt/CB, and SnO_2/CB electrodes in an Ar-saturated 0.5 M H_2SO_4 solution at 30 °C. A couple of peaks due to hydrogen adsorption and desorption on the Pt surface [31] were observed for $Pt/SnO_2(9:1)/CB$, $Pt/SnO_2(3:1)/CB$ and $Pt/SnO_2(1:1)/CB$ electrodes as well as a Pt/CB electrode. However, the hydrogen adsorption/desorption peaks were indistinct, as described previously for Nafion-coated Pt nanoparticles/CB [10,32] and PtSn/CB electrodes [10]. The $Pt/SnO_2(1:3)/CB$ electrode did not have distinct hydrogen adsorption/desorption peaks. The electrochemically active surface area (EASA) of the Pt nanoparticles was evaluated from the electric charge of the hydrogen desorption wave in each CV, supposing 210 $\mu C\,cm^{-2}$ for polycrystalline Pt. EASA was 0.208, 0.305, 0.197, and 0.284 cm^2 for $Pt/SnO_2(9:1)/CB$, $Pt/SnO_2(3:1)/CB$, $Pt/SnO_2(1:1)/CB$, and Pt/CB electrodes, respectively.

Fig. 6 shows linear sweep voltammograms for $Pt/SnO_2(9:1)/CB$, $Pt/SnO_2(3:1)/CB$, $Pt/SnO_2(1:1)/CB$, $Pt/SnO_2(1:3)/CB$, Pt/CB, and SnO_2/CB electrodes in an Ar-saturated 0.5 M H_2SO_4 solution containing 1 M ethanol. The specific activity (SA), defined as the current density per real Pt surface area, was used. Fig. 6 shows that the onset potential of EOR shifts toward a less positive value when the Pt/Sn ratio increases up to 3. The onset potential for the $Pt/SnO_2(3:1)/CB$ electrode (*ca.* 0.15 V) was *ca.* 0.25 V less positive than that for the Pt/CB electrode (*ca.* 0.40 V), suggesting that the former had smaller overpotential for EOR than the latter. These results clearly indicate that SnO_2 synergistically enhances the EOR activity of Pt. In addition, the $Pt/SnO_2(3:1)/CB$ electrode exhibited smaller overpotential for EOR than that of bimetallic Pt–Sn/CB [14], $Pt/SnO_x/CB$ [33], and Pt microparticles dispersed on SnO_2 thin films [34]. Therefore, we can conclude that the combination of Pt and SnO_2 nanoparticles provides the highest EOR activity for Pt/Sn catalysts.

SAs for EOR were plotted against mole fraction of Pt (x_{Pt}) at 0.4 and 0.6 V in Fig. 7. The $Pt/SnO_2(3:1)/CB$ electrode whose x_{Pt} was 0.79 displayed the highest SAs (0.51 and 0.86 mA Pt-cm^{-2}

Table 1
Typical properties of $Pt/SnO_2/CB$ prepared with different SnO_2 contents and Pt/CB and SnO_2/CB catalysts.

Catalysts	Content Pt:SnO_2/at.%	d_{XRD}[a]/nm		d_{TEM}[b]/nm	
		Pt	SnO_2	Pt	SnO_2
Pt/CB	100:0	3.6	–	2.4 ± 0.6	–
$Pt/SnO_2(9:1)/CB$	82:18	3.4	–	–	–
$Pt/SnO_2(3:1)/CB$	71:29	2.9	–	3.1 ± 0.5	2.5 ± 0.3
$Pt/SnO_2(1:1)/CB$	46:54	2.8	2.5	3.0 ± 0.5	2.6 ± 0.3
$Pt/SnO_2(1:3)/CB$	27:73	–	–	2.8 ± 0.5	2.5 ± 0.3
SnO_2/CB	0:100	–	2.0	–	2.0

[a] Average crystallite size calculated from Scherrer's equation.
[b] Average particle size based on TEM observation.

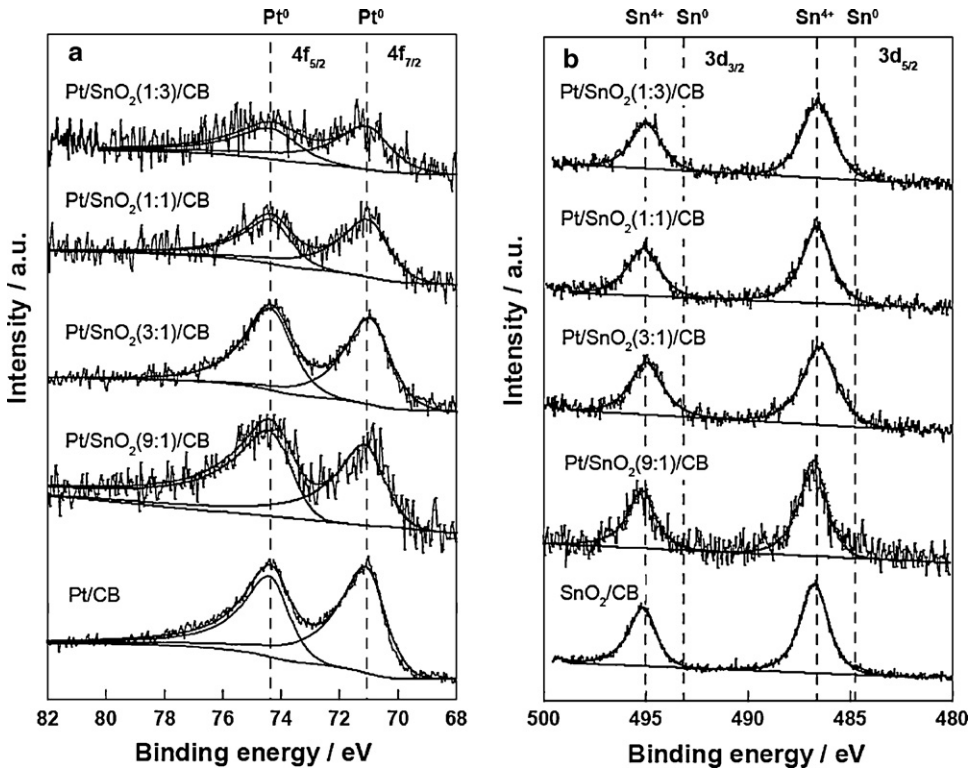

Fig. 4. (a) Pt4f and (b) Sn3d core level spectra for $Pt/SnO_2(9:1)/CB$, $Pt/SnO_2(3:1)/CB$, $Pt/SnO_2(1:1)/CB$, $Pt/SnO_2(1:3)/CB$, and Pt/CB catalysts.

at 0.4 and 0.6 V, respectively). The SAs at 0.4 and 0.6 V for the $Pt/SnO_2(3:1)/CB$ electrode were *ca*. 25 and 4 times higher than those for the Pt/CB electrode, respectively. In addition, the SA at 0.4 V for the $Pt/SnO_2(3:1)/CB$ electrode was still higher than that for PtSn [15], PtSnIr [35], and PtMo [36] which showed high EOR activities. The $Pt/SnO_2(1:1)/CB$ electrode, which had the same real surface area as the Pt/CB electrode, also had higher SAs than the Pt/CB electrode. On the other hand, the EOR activity of the $Pt/SnO_2(1:3)/CB$ electrode was lower than that of the Pt/CB electrode probably because the content of SnO_2 with poor electronic conductivity increased [35]. The SnO_2/CB electrode was inactive for EOR.

Synergistic effect arising from the combination of Pt and SnO_2 nanoparticles can be ascribed to the bifunctional mechanism [15,37,38] in which Sn atoms adjacent to Pt atoms supply oxygen-containing species for the oxidative removal of Pt-bound CO-like intermediates. The $Pt/SnO_2(3:1)/CB$ electrode, which displayed the highest SA, seems to have the optimal number of Pt and Sn pairs to accelerate the oxidative removal.

Fig. 8 shows CO-stripping voltammograms of $Pt/SnO_2(3:1)/CB$, $Pt/SnO_2(1:1)/CB$, and Pt/CB electrodes. For the Pt/CB electrode, the onset potential of CO oxidation was *ca.* 0.6 V, and the sharp oxidation peak was observed at *ca*. 0.9 V. On the other hand, the CO oxidation peak for the $Pt/SnO_2(3:1)/CB$ and $Pt/SnO_2(1:1)/CB$ electrodes were broad and split into two. Moreover, the CO-stripping voltammograms for the $Pt/SnO_2(3:1)/CB$, $Pt/SnO_2(1:1)/CB$ and Pt/CB electrodes were similar to those reported by Eguchi and co-workers [39] and Ueda and co-workers [40]. In the case of the $Pt/SnO_2(3:1)/CB$ electrode, the peak at the higher potential (0.82 V) is attributed to CO oxidation on Pt atoms, while the shoulder at the lower potential (0.3–0.7 V) is assigned to that on Pt atoms adja-

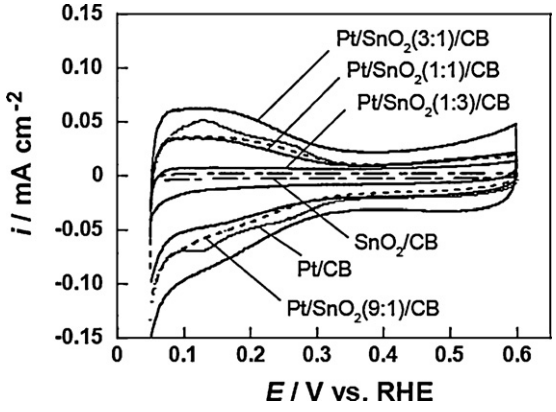

Fig. 5. Cyclic voltammograms of Nafion-coated $Pt/SnO_2(9:1)/CB$, $Pt/SnO_2(3:1)/CB$, $Pt/SnO_2(1:1)/CB$, $Pt/SnO_2(1:3)/CB$, Pt/CB, and SnO_2/CB electrodes in an Ar-saturated 0.5 M H_2SO_4 solution at 30 °C. Sweep rate = 20 mV s^{-1}.

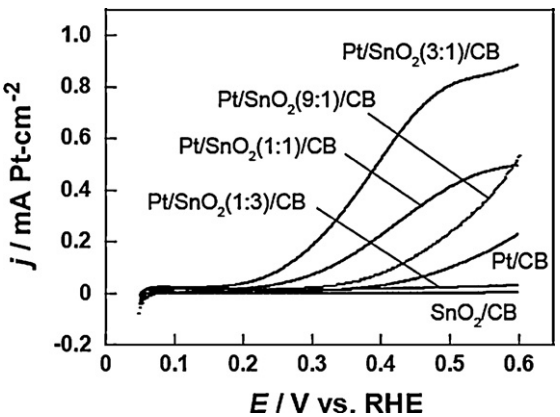

Fig. 6. Specific EOR activity of Nafion-coated $Pt/SnO_2(9:1)/CB$, $Pt/SnO_2(3:1)/CB$, $Pt/SnO_2(1:1)/CB$, $Pt/SnO_2(1:3)/CB$, Pt/CB, and SnO_2/CB electrodes in Ar-saturated (1 M C_2H_5OH + 0.5 M H_2SO_4) solution at 30 °C. Sweep rate = 20 mV s^{-1}. w_{Pt/SnO_2} = 12.8 μg cm^{-2}, w_{CB} = 5.5 μg cm^{-2}.

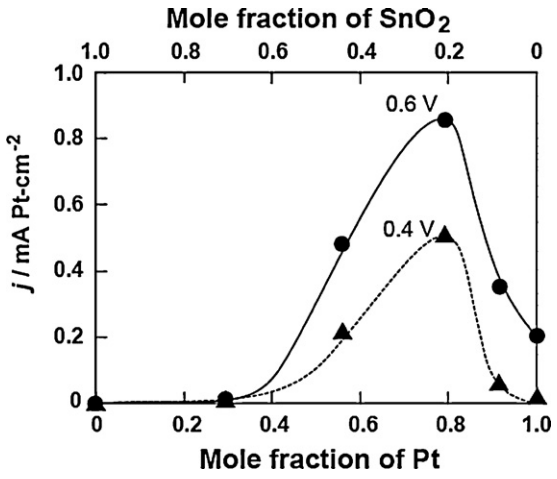

Fig. 7. Specific EOR activity at 0.4 and 0.6 V for Nafion-coated Pt/SnO_2(9:1)/CB, Pt/SnO_2(3:1)/CB, Pt/SnO_2(1:1)/CB, Pt/SnO_2(1:3)/CB, Pt/CB, and SnO_2/CB electrodes in Ar-saturated (1 M C_2H_5OH + 0.5 M H_2SO_4) solution at 30 °C. Sweep rate = 20 mV s^{-1}. $w_{Pt/SnO_2} = 12.8\ \mu g\ cm^{-2}$, $w_{CB} = 5.5\ \mu g\ cm^{-2}$.

cent to Sn atoms. This indicates that in the latter, overpotential for CO oxidation is lowered via the bifunctional mechanism. The similar results were obtained for the Pt/SnO_2(1:1)/CB electrode. Moreover, the CO oxidation current at the Pt/SnO_2(3:1)/CB electrode was higher than that at the Pt/SnO_2(1:1)/CB electrode, which is attributable to the difference in the bifunctional effect based on the number of Pt and Sn pairs.

Fig. 9 shows time courses of current density during EOR at 0.4 and 0.6 V for Pt/SnO_2(3:1)/CB and Pt/CB electrodes in Ar-saturated (1 M C_2H_5OH + 0.5 M H_2SO_4) solutions at 30 °C. Table 2 shows SAs at the beginning, 60 and 180 min in potentiostatic electrolyses at 0.4 and 0.6 V for each electrode. The decay of oxidation current density at 0.6 V was suppressed more significantly than that at 0.4 V. In addition, the oxidation current density at the Pt/SnO_2(3:1)/CB electrode decayed more slowly than that at the Pt/CB electrode, indicating clearly that the Pt/SnO_2(3:1)/CB electrode was superior in durability to the Pt/CB electrode.

Fig. 10 shows CVs of a Nafion-coated Pt/SnO_2(3:1)/CB electrode in an Ar-saturated 0.5 M H_2SO_4 solution at 30 °C. In the CV at the 1st potential sweep, two couples of peaks due to hydrogen adsorption/desorption on the Pt surface [31] at potentials less than 0.3 V and Sn(II)/Sn(IV) redox reactions at *ca.* 0.6 and *ca.* 0.8 V were observed. The former current density gradually increased with an increase in sweep number, while the latter one decreased. In the CV at 20th cycle, the peaks due to Sn(II)/Sn(IV) redox reactions at *ca.* 0.6 and *ca.* 0.8 V disappeared and typical distinct peaks due to hydrogen adsorption/desorption on the Pt surface were observed, indicating clearly that SnO_2 on Pt easily dissolved out during the redox reactions and the increase in the EASA of Pt originates from the disappearance of SnO_2 on Pt.

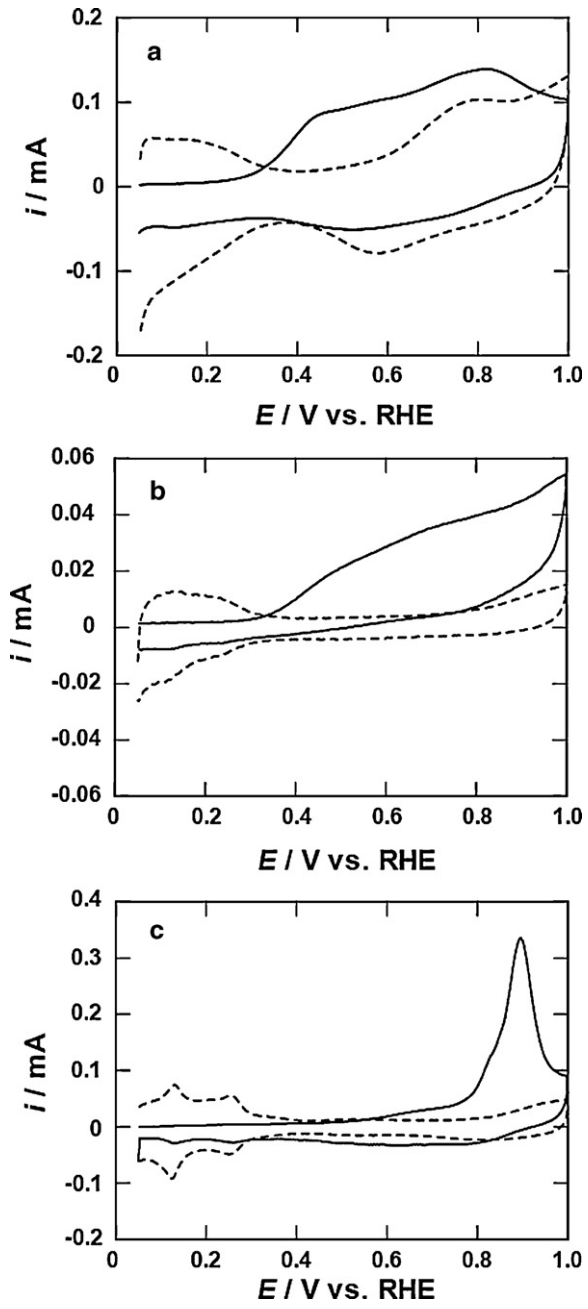

Fig. 8. CO-stripping voltammograms for Nafion-coated (a) Pt/SnO_2(3:1)/CB, (b) Pt/SnO_2(1:1)/CB, and (c) Pt/CB catalysts in 0.5 M H_2SO_4 solution at 30 °C. Sweep rate = 50 mV s^{-1}. $w_{Pt/SnO_2} = 12.8\ \mu g\ cm^{-2}$, $w_{CB} = 5.5\ \mu g\ cm^{-2}$.

Table 2
Durability of Pt/SnO_2(3:1)/CB and Pt/CB electrodes.

E/V	Catalyst	Current density/mA Pt-cm^{-2}			$i_{(60-180)}$[a]/%
		Beginning	60 min (i_{0-60})[b]	180 min (i_{0-180})[c]	
0.4	Pt/SnO_2(3:1)/CB	0.587	0.126 (22%)	0.090 (15%)	71
	Pt/CB	0.009	*ca.* 0 (0%)	*ca.* 0 (0%)	*ca.* 0
0.6	Pt/SnO_2(3:1)/CB	1.534	0.615 (40%)	0.459 (30%)	75
	Pt/CB	0.272	0.086 (32%)	0.046 (17%)	53

[a] $i_{180}/i_{60} \times 100$.
[b] $i_{60}/i_0 \times 100$.
[c] $i_{180}/i_0 \times 100$.

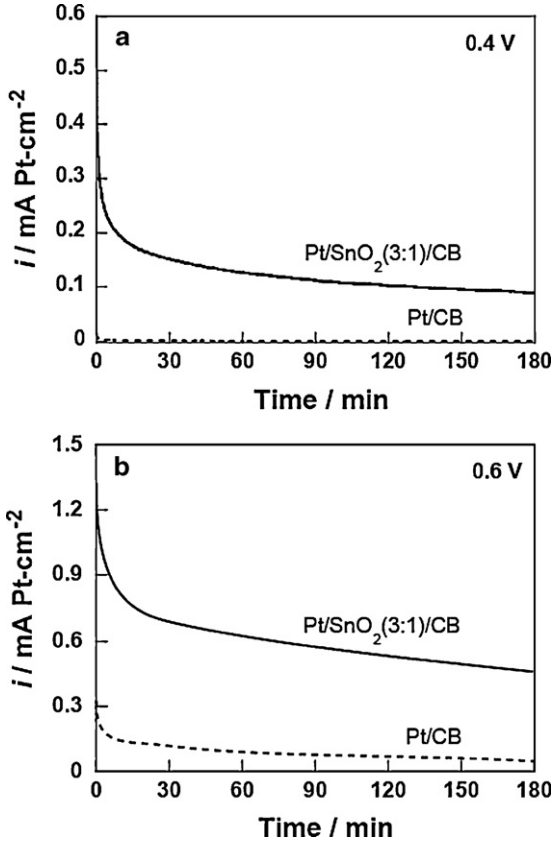

Fig. 9. Time courses of current density at (a) 0.40 and (b) 0.60 V for Nafion-coated $Pt/SnO_2(3:1)/CB$ and Pt/CB electrodes in Ar-saturated (1 M C_2H_5OH + 0.5 M H_2SO_4) solution at 30 °C. $w_{Pt/SnO_2} = 12.8\,\mu g\,cm^{-2}$, $w_{CB} = 5.5\,\mu g\,cm^{-2}$.

On the other hand, as shown in Fig. 11, CV at the SnO_2/CB electrode was almost identical for 20 cycles, and current density in the CV was much smaller than that for the $Pt/SnO_2(3:1)/CB$ electrode. Moreover, the redox peaks of Sn(II)/Sn(IV) at *ca.* 0.6 and *ca.* 0.8 V were not observed even in the CV at the 1st cycle, suggesting that the degree of dispersion of SnO_2 nanoparticles on CB was low compared to the $Pt/SnO_2(3:1)/CB$. This might make the dissolution of SnO_2 with low electronic conductivity difficult.

The SnO_2 on Pt causes underestimation of the EASA of Pt. The SnO_2 coverage on the Pt surface (θ_{SnO_2}) in $Pt/SnO_2(3:1)/CB$ can be

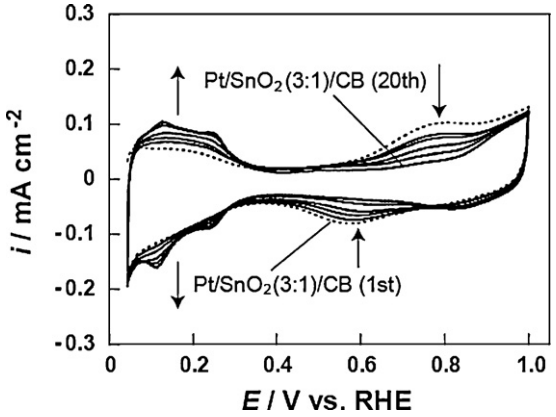

Fig. 10. Cyclic voltammograms of Nafion-coated $Pt/SnO_2(3:1)/CB$ electrode in Ar-saturated 0.5 M H_2SO_4 solution at 30 °C. Sweep rate = 20 mV s^{-1}. $w_{Pt/SnO_2} = 12.8\,\mu g\,cm^{-2}$, $w_{CB} = 5.5\,\mu g\,cm^{-2}$.

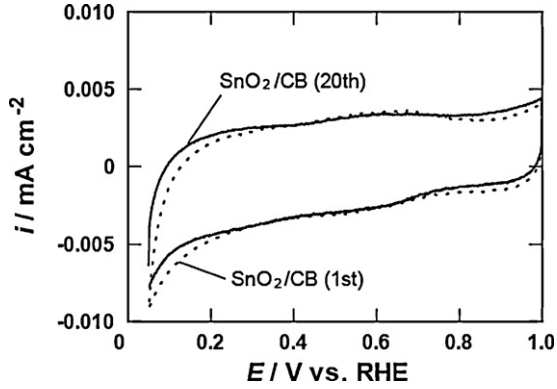

Fig. 11. Cyclic voltammograms of Nafion-coated SnO_2/CB electrode in Ar-saturated 0.5 M H_2SO_4 solution at 30 °C. Sweep rate = 20 mV s^{-1}. $w_{Pt/SnO_2} = 12.8\,\mu g\,cm^{-2}$, $w_{CB} = 5.5\,\mu g\,cm^{-2}$.

calculated by the following equation:

$$\theta_{SnO_2} = \frac{1 - Q_{H(Pt/SnO_2)}}{Q_{H(Pt)}} \quad (1)$$

where $Q_{H(Pt/SnO2)}$ and $Q_{H(Pt)}$ are EASAs evaluated from the CVs at 1st and 20th cycles, respectively. The θ_{SnO_2} was evaluated to be 0.47, indicating that many pairs of Pt and Sn are formed and cause the synergistic effect.

Using the $Pt/SnO_2(3:1)/CB$ electrode, electrolysis at 0.6 V was performed for 16 h (0.696 C). Acetic acid, acetaldehyde, and CO_2 can be produced by EOR. The products were analyzed by HPLC and GC after the potentiostatic electrolysis. The predominant reaction product was acetic acid, which was also the main product in EOR using other Pt- and Sn-containing electrocatalysts [41], but acetaldehyde was not detected. The current efficiencies for acetic acid and CO_2 production were about 69.0 (1.25 μmol) and 26.6% (0.185 μmol), respectively. Vigier et al. reported that the first product of the dissociative adsorption of ethanol on Pt surface was acetaldehyde, which only requires the transfer of 2 electrons per ethanol molecule, and in the second step acetaldehyde was oxidized to acetic acid and CO_2 [41]. Adzic and co-workers have recently reported that Pt–Rh–SnO_2 catalyst was effective for the oxidation of ethanol to CO_2 with selectivity over 90% [42]. The addition of a third element like Rh into the $Pt/SnO_2(3:1)/CB$ catalyst may enable a complete EOR to CO_2. Further studies are now in progress to investigate this idea.

4. Conclusions

We prepared Pt/SnO_2/CB catalysts with different Pt and SnO_2 contents by the modified Bönnemann method. TEM images of the $Pt/SnO_2(3:1)/CB$ catalyst showed twin Pt and SnO_2 nanoparticles with Pt(1 1 1) and SnO_2(1 1 0) lattice fringes. The average size of Pt and SnO_2 nanoparticles were 3.0 ± 0.5 and 2.6 ± 0.3 nm, respectively, for $Pt/SnO_2(1:1)/CB$ and 2.8 ± 0.5 and 2.5 ± 0.3 nm, respectively, for $Pt/SnO_2(1:3)/CB$. Pt4f and Sn3d core level spectra of $Pt/SnO_2(3:1)/CB$, $Pt/SnO_2(1:1)/CB$, $Pt/SnO_2(1:3)/CB$, and Pt/CB catalysts showed that Pt^0 and Sn^{4+} or SnO_2 were observed at the surface, suggesting that Sn was oxidized to SnO_2. The onset potential of EOR for the $Pt/SnO_2(3:1)$/electrode in an Ar-saturated 0.5 M H_2SO_4 solution containing 1 M C_2H_5OH was about 0.25 V less positive than that for the Pt/CB electrode. In addition, the SAs at 0.4 and 0.6 V for $Pt/SnO_2(3:1)/CB$ were *ca.* 25 and 4 times higher than those for the Pt/CB electrode, respectively, indicating that EOR activity was significantly improved because of the synergistic effect of Pt and SnO_2. $Pt/SnO_2(3:1)/CB$ and $Pt/SnO_2(1:1)/CB$ catalysts showed a CO oxidation peak at *ca.* 0.8 V, which was attributed to the CO

oxidation on Pt, and a shoulder at *ca.* 0.4 V, which was ascribed to CO oxidation on Pt adjacent to Sn atoms. This indicates that contact with SnO_2 can lower the oxidation potential of Pt-adsorbed CO via a bifunctional mechanism. Time course of the current density at 0.40 and 0.60 V vs. RHE for Pt/SnO_2(3:1)/CB decayed more slowly than that for the Pt/CB electrode. The Pt/SnO_2(3:1)/CB electrode therefore displayed significantly improved EOR activity and durability compared with the Pt/CB electrode. The main product of EOR was acetic acid. The current efficiency for acetic acid production was about 70% while that of CO_2 was about 30%.

Acknowledgments

This work was partly supported by Grant-in-Aid for Young Scientists (B) (No. 19750170) from the Ministry of Education, Culture, Sports, Science and Technology of Japan.

References

[1] S. Wasmus, A. Küver, J. Electroanal. Chem. 461 (1999) 14.
[2] X. Ren, P. Zelenay, S. Thomas, J. Davey, S. Gottesfeld, J. Power Sources 86 (2000) 111.
[3] D. Chu, S. Gilman, J. Electrochem. Soc. 141 (1994) 1770.
[4] E. Higuchi, N. Asano, K. Miyatake, H. Uchida, M. Watanabe, Electrochim. Acta 52 (2007) 5272.
[5] C. Lamy, A. Lima, V. LeRhun, F. Delime, C. Coutanceau, J.M. Léger, J. Power Sources 105 (2002) 283.
[6] A.O. Neto, M.J. Giz, J. Perez, E.A. Ticianelli, E.R. Gonzalez, J. Electrochem. Soc. 149 (2002) A272.
[7] J. Mann, N. Yao, A.B. Bocarsly, Langmuir 22 (2006) 10432.
[8] L. Dubau, F. Hahn, C. Coutanceau, J.M. Léger, C. Lamy, J. Electroanal. Chem. 554–555 (2003) 407.
[9] J.P.I. de Souza, S.L. Queiroz, K. Bergamaski, E.R. Gonzalez, F.C. Nart, J. Phys. Chem. B 106 (2002) 9825.
[10] F. Vigier, C. Coutanceau, F. Hahn, E.M. Belgsir, C. Lamy, J. Electroanal. Chem. 563 (2004) 81.
[11] H. Wang, Z. Jusys, R.J. Behm, J. Phys. Chem. B 108 (2004) 19413.
[12] H.B. Suffredini, V. Tricoli, L.A. Avaca, N. Vatistas, Electrochem. Commun. 6 (2004) 1025.
[13] Y. Bai, J. Wu, J. Xi, J. Wang, W. Zhu, L. Chen, X. Qiu, Electrochem. Commun. 7 (2005) 1087.
[14] C. Lamy, S. Rousseau, E.M. Belgsir, C. Coutanceau, J.M. Léger, Electrochim. Acta 49 (2004) 3901.
[15] J. Ribeiro, D.M. dos Anjos, K.B. Kokoh, C. Coutanceau, J.-M. Léger, P. Olivi, A.R. de Andrade, G. Tremiliosi-Filho, Electrochim. Acta 52 (2007) 6997.
[16] M. Min, J. Cho, K. Cho, H. Kim, Electrochim. Acta 45 (2000) 4211.
[17] L. Xiong, A. Manthiram, Electrochim. Acta 50 (2005) 2323.
[18] J.R.C. Salgado, E. Antolini, E.R. Gonzalez, J. Electrochem. Soc. 151 (2004) A2143.
[19] M.K. Ravikumar, A.K. Shukla, J. Electrochem. Soc. 143 (1996) 2601.
[20] W. Li, W. Zhou, H. Li, Z. Zhou, B. Zhou, G. Sun, Q. Xin, Electrochim. Acta 49 (2004) 1045.
[21] E.V. Spinacé, A.O. Neto, T.R.R. Vasconcelos, M. Linardi, J. Power Sources 137 (2004) 17.
[22] S. Sun, S. Andersw, T. Thomson, J.E.E. Baglin, M.F. Toney, H.F. Hamann, C.B. Murray, B.D. Terris, J. Phys. Chem. B 107 (2003) 5419.
[23] H. Bönnemann, R.M. Richards, Eur. J. Inorg. Chem. (2001) 2455.
[24] H. Bönnemann, W. Brijoux, B. Korall, Angew. Chem. Int. Ed. Engl. 30 (1991) 1312.
[25] H. Bönnemann, P. Britz, W. Vogel, Langmuir 14 (1998) 6654.
[26] R. Burch, Phys. Chem. Chem. Phys. 8 (2006) 5483.
[27] Q. Fu, H. Saltsburg, M. Flytzani-Stephanopoulos, Science 301 (2003) 935.
[28] J.A. Rodriguez, S. Ma, P. Liu, J. Hebek, J. Evans, M. Perez, Science 318 (2007) 1757.
[29] E. Higuchi, H. Uchida, M. Watanabe, J. Electroanal. Chem. 583 (2005) 69.
[30] J. Cao, C. Du, S.C. Wang, P. Mercier, X. Zhang, H. Yang, D.L. Akins, Electrochem. Commun. 9 (2007) 735.
[31] K.W. Park, J.H. Choi, B.K. Kwon, S.A. Lee, Y.E. Sung, H.Y. Ha, S.A. Hong, H. Kim, A. Wieckowski, J. Phys. Chem. B 106 (2002) 1869.
[32] H. Yano, J. Inukai, H. Uchida, M. Watanabe, K.B. Panakkattu, T. Kobayashi, J.H. Chung, E. Oldfield, A. Wieckowski, Phys. Chem. Chem. Phys. 8 (2006) 4932.
[33] L. Jiang, L. Colmenares, Z. Jusys, G.Q. Sun, R.J. Behm, Electrochim. Acta 53 (2007) 377.
[34] A.L. Santos, D. Profeti, P. Olivi, Electrochim. Acta 50 (2005) 2615.
[35] D.M.D. Anjos, K.B. Kokoh, J.M. Léger, A.R.D. Andrade, P. Olivi, G. Tremiliosi-Filho, J. Appl. Electrochem. 36 (2006) 1391.
[36] M. Nakada, A. Ishihara, S. Mitsushima, N. Kamiya, K. Ota, Electrochem. Solid State Lett. 10 (2007) F1.
[37] J.L. Margitfalvi, I. Bortáth, M. Hegadus, A. Szegedi, Catal. Today 73 (2002) 343.
[38] M. Watanabe, S. Motoo, J. Electroanal. Chem. Interfacial Chem. 60 (1975) 267.
[39] T. Matsui, K. Fujiwara, T. Okanishi, R. Kikuchi, T. Takeguchi, K. Eguchi, J. Power Sources 155 (2006) 152.
[40] G. Wang, T. Takeguchi, T. Yamanaka, E.N. Muhamad, M. Mastuda, W. Ueda, Appl. Catal. B 98 (2010) 86.
[41] F. Vigier, S. Rousseau, C. Coutanceau, Jean-Michel Leger, C. Lamy, Top. Catal. 40 (2006) 111.
[42] A. Kowal, M. Li, M. Shao, K. Sasaki, M.B. Vukmirovic, J. Zhang, N.S. Marinkovic, P. Liu, A.I. Frenkel, R.R. Adzic, Nat. Mater. 8 (2009) 325.